Science of the Total Environment 612 (2018) 975–984

Contents lists available at ScienceDirect

Science of the Total Environment

journal homepage: www.elsevier.com/locate/scitotenv

Characteristics of air pollution in different zones of Sichuan Basin, China

Guicai Ning [a], Shigong Wang [b,a,*], Minjin Ma [a], Changjian Ni [b], Ziwei Shang [a], Jiaxin Wang [b], Jingxin Li [c]

[a] The Gansu Key Laboratory of Arid Climate Change and Reducing Disaster, College of Atmospheric Sciences, Lanzhou University, Lanzhou 730000, China
[b] Mountain Environment and Meteorology Key Laboratory of Education Bureau of Sichuan Province, College of Atmospheric Sciences, Chengdu University of Information Technology, Chengdu 610225, China
[c] Institute of Climate System, Chinese Academy of Metrological Sciences, Beijing 100081, China

HIGHLIGHTS

- Air pollution was studied in the bottom, slope and edge zone of Sichuan Basin.
- Variations of $PM_{2.5}$ and PM_{10} concentrations with altitude can be fitted by $y = (a + b / x)^2$.
- Horizontal homogeneities of $PM_{2.5}$ and PM_{10} are strong in the bottom of the basin.
- Gaseous pollutant concentrations exhibited diverse variations with altitude.

GRAPHICAL ABSTRACT

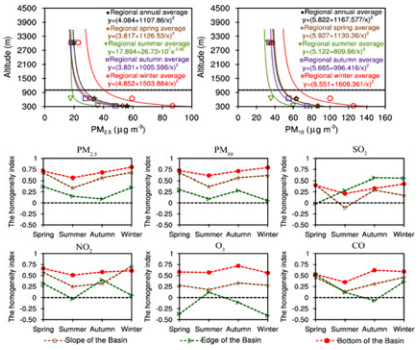

ARTICLE INFO

Article history:
Received 4 July 2017
Received in revised form 17 August 2017
Accepted 20 August 2017
Available online 6 September 2017

Editor: D. Barcelo

Keywords:
Sichuan Basin
Particulate matter
Gaseous pollutants
Temporal-spatial variation

ABSTRACT

Sichuan Basin, located in southwest China, has been ranked as the fourth of heavily air polluted regions in China partly due to its deep mountain-basin topography. However, spatial-temporal distribution of air pollution over the basin is still unclear due to the lack of monitoring data and poor knowledge. Since January 2015, six criteria air pollutants began to be monitored in 20 cities across the basin. The measured data enable us to analyze the basin-wide spatial-temporal distribution characteristics of these air pollutants. Results revealed heavy air pollution in the bottom zone, medium in the slope zone, and light pollution in the edge zone of the Basin in terms of the altitudes of air quality monitoring stations across the Basin. The average concentrations of $PM_{2.5}$ and PM_{10} were 55.87 μg/m^3 and 86.49 μg/m^3 in the bottom, 33.76 μg/m^3 and 63.33 μg/m^3 in the slope, and 19.71 μg/m^3 and 35.06 μg/m^3 in the edge, respectively. In the bottom and slope of the basin, high $PM_{2.5}$ concentration events occurred most frequently in winter. While in summer, ozone became primary pollutant. Among the six air pollutants, concentrations of $PM_{2.5}$ and PM_{10} decrease dramatically with increasing altitude which was fitted by a nonlinear relationship between particulate matter (PM) concentrations and altitude. This relationship was validated by extinction coefficient profiles from CALIPSO observations and EV-lidar data, and hence used to reflect vertical distribution of air PM concentrations. It has been found that the thickness of higher PM concentrations is less than 500 m in the basin. In the bottom of the basin, PM concentrations exhibited stronger horizontal homogeneities as compared with those in the North China Plain and Yangtze River Delta. However, gaseous pollutants seemed not to show clear relationships between their concentrations and altitudes in the basin. Their horizontal homogeneities were less significant compared to PM.

* Corresponding author at: College of Atmospheric Sciences, Lanzhou University, 730000 Lanzhou, Gansu, China.
E-mail addresses: ninggc15@lzu.edu.cn (G. Ning), wangsg@cuit.edu.cn, wangsg@lzu.edu.cn (S. Wang), minjinma@lzu.edu.cn (M. Ma), lijingxin@camscma.cn (J. Li).

http://dx.doi.org/10.1016/j.scitotenv.2017.08.205
0048-9697/

1. Introduction

With rapid economic development and urbanization acceleration in China, urban air pollution becomes a serious problem due to a significant increase in air pollutant emissions (Brauer et al., 2012; Fang et al., 2009; Li et al., 2017). Although the excessive emission is a key factor to cause heavy air pollution, local complex terrain and meteorological conditions also play a very important role on regional air quality (Deng et al., 2014; Hu et al., 2014; Tao et al., 2014). It has been widely noticed that heavy air pollution events often take place in mountainous (basin) cities (Boznar et al., 1993; Gustin et al., 2015; Jazcilevich et al., 2005; Saide et al., 2011). Heavy air pollutions occurring in many cities of China, such as Taiyuan, Beijing, Hong Kong, and Lanzhou, were significantly affected by mountain-valley topography (He et al., 2015; Miao et al., 2015; Yim et al., 2014; Zhao et al., 2015). Complex terrain and special local meteorological conditions have been also observed to be conducive to worsen regional air quality in the Sichuan Basin which is now ranked as the fourth of heavily polluted regions in China following Beijing-Tianjin-Hebei region, the Yangtze River Delta, and the Pearl River Delta (Zhang et al., 2012). However, the spatial-temporal distribution characteristics of air pollution in the basin are still unclear due to the lack of monitoring data and limited researches.

Sichuan Basin is a large deep basin with 20 cities including two mega cities Chengdu and Chongqing. The Basin is characterized by high population densities, a large amount of motor vehicles, and rapidly developed industrialization. The gross domestic product (GDP) of the 20 cities during 2015 is about 670.1 billion US dollars. Because of the large amount of energy consumption and anthropogenic emissions, the air quality in the basin has been worsening over the past decades (Chen et al., 2014). Under the effects of the particular topography of Sichuan Basin, the air temperature drops slowly in night which causes small temperature gradient between the daytime and nighttime. Low wind speed throughout a year is beneficial to the occurrence of air stagnation (Chen and Xie, 2012; Huang et al., 2017; Wang et al., 2017). Tibetan Plateau and Yunnan-Guizhou Plateau force a unique atmospheric circulation in the Basin (Wang and Tan, 2014; Yu et al., 2016), resulting in high humidity and frequent occurrence of fog which favor the formation and growth of particulate matter (PM) (Luo Yunfeng et al., 2000; Niu et al., 2010). Heavy emissions, particular topography, and unique atmospheric circulation all together cause the heavy wintertime fine particle pollution over the basin (Liao et al., 2017; Tao et al., 2013a) which is now one of the most heavily contaminated regions by $PM_{2.5}$ (Battelle Memorial Institute and Center for International Earth Science Information Network - CIESIN - Columbia University, 2013). In summer, surface ozone becomes primary air pollutant over the Basin.

Fine particles and toxic gaseous pollutants can cause respiratory diseases, cardiovascular diseases, and lung cancer (Guo et al., 2016; Langrish et al., 2012; Pope and Dockery, 2006). Due to heavy air pollution across the Basin, there is an urgent need to investigate the spatial and temporal distribution of air pollutants over the Basin. Previous studies for air pollution were mostly performed in the two megacities Chengdu and Chongqing located in the bottom of the basin (Chen et al., 2017; Li et al., 2015; Zhang et al., 2017) because of sparse measurements in other places of the Basin.

Since January 2015, the real-time hourly concentrations of sulfur dioxide (SO_2), nitrogen dioxide (NO_2), particulate matter with aerodynamic diameter equal to or less than 10 μm (PM_{10}), $PM_{2.5}$, carbon monoxide (CO), 1 h mean ozone (O_3) and 8 h mean O_3 began to be routinely monitored by Chinese Ministry of Environmental Protection (MEP) in 20 cities of the Sichuan Basin. The monitoring program covers all prefecture-level cities of the Basin. These data enable us to examine the changes in sampled air pollutants with altitudes of the Basin and their horizontal homogeneities. The extinction coefficient profiles from CALIPSO observations and the EV-lidar in Chengdu were used to verify the vertical distribution of PM concentrations. The objective of this article is to explore the distribution of air pollution in a three-dimensional space of the Basin and its temporal variation.

2. Methods and data

2.1. Description of study areas and methods

Located in the east of the Tibetan Plateau, the maximum depth of the Sichuan Basin is more than 2000 m. The Basin is surrounded by Daba and Qinling Mountains to the north, Yunnan-Guizhou Plateau to the south, and Wushan Mountains to the east (Fig. 1). Low wind speed and frequent temperature inversion prevail in winter due to Basin's topography forcing (Chen and Xie, 2012; Li et al., 2015; Yu et al., 2016). The unique meteorological conditions in the basin lead air pollution mechanism to be distinctive from other places of China (Chen et al., 2014).

A total of 20 cities in the Basin are selected and categorized into three zones in terms of their respective altitude and terrain characteristics. These are the bottom zone, slope zone, and edge zone. Fifteen cities, Chengdu (CD), Zigong (ZG), Meishan (MS), Luzhou (LZ), Deyang (DY), Neijiang (NJ), Leshan (LS), Dazhou (DZ), Yibin (YB), Nanchong (NC), Ziyang (ZY), Guangan (GA), Suining (SN), Chongqing (CQ) and Mianyang (MY) are located in the bottom zone. Three cities, Yaan (YA), Bazhong (BZ) and Guangyuan (GY) are located in the slope zone. The other two cities Ganzizhou (GZZ) and Abazhou (ABZ) are located in the edge zone. Air pollutions in the three zones are comparatively analyzed to elucidate their characteristics of spatial and temporal distribution.

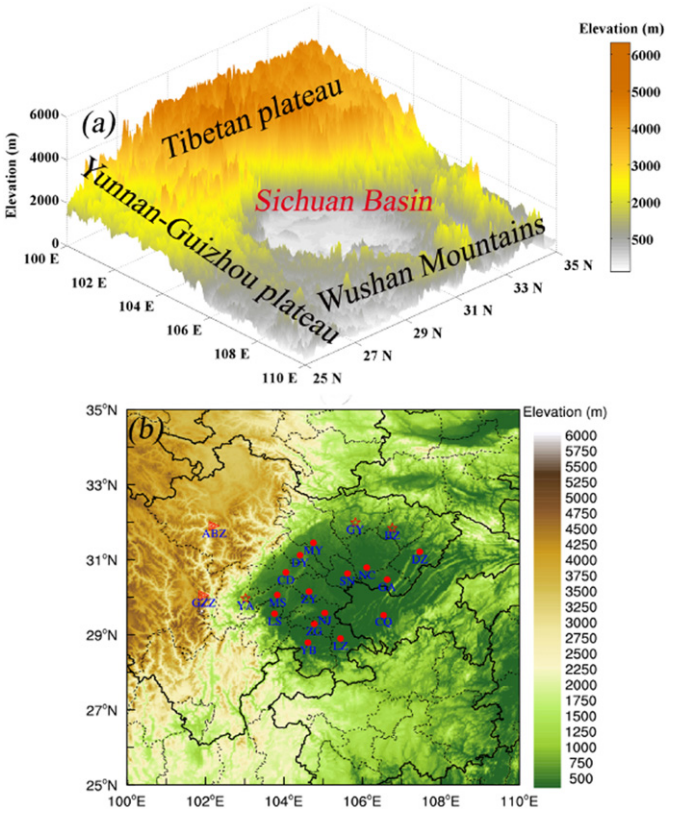

Fig. 1. (a) Three-dimensional terrain in the Sichuan Basin and its surrounding areas; (b) locations of the cities in the basin (the cities in the bottom zone of the Basin are marked with red solid dots, the cities in the slope zone are marked with red five-pointed stars, and the cities in the edge zone are marked with red triangles).

2.2. Data

2.2.1. Air pollutants

Hourly concentrations of six pollutants ($PM_{2.5}$, PM_{10}, SO_2, NO_2, CO, 1 h O_3 and 8 h O_3) and the air quality daily reports from January 1st, 2015 to December 31st, 2016 in the 20 selected cities were used in the statistical analysis for the characteristics of air pollutants' spatial-temporal distribution in the three zones of the Basin. To compare the differences of horizontal homogeneities of $PM_{2.5}$ and PM_{10} concentrations between the Basin and the North China Plain (NCP) as well as the Yangtze River Delta (YRD), we also collected the hourly concentration data of $PM_{2.5}$ and PM_{10} in 13 cities (Beijing, Langfang, Tianjin, Baoding, Tangshan, Cangzhou, Hengshui, Shijiazhuang, Qinhuangdao, Jinan, Handan, Qingdao and Zhengzhou) of NCP, and in 17 cities (Shanghai, Jiaxing, Nantong, Huzhou, Shaoxing, Hangzhou, Taizhoushi, Yangzhou, Nanjing, Jinhua, Lishui, Huaian, Quzhou, Wenzhou, Suqian, Lianyungang and Xuzhou) of YRD, respectively. In the statistical analysis, if the daily concentration of one of the six air pollutants exceeds CAAQS (Chinese Ambient Air Quality Standards (GB3095-2012)) Grade II standards, this day is regarded as a non-attainment day (Liu et al., 2013; Wang et al., 2014; Xu et al., 2016). The daily air quality reports were collected from the MEP website (http://datacenter.mep.gov.cn/index). The MEP hourly concentrations data were collected at the website (http://113.108.142.147:20035/emcpublish/). Eight-hour mean O_3 concentrations were calculated based on hourly O_3 concentrations. All the measurements were conducted at the national air quality monitoring sites located in each city. Multiple air quality monitoring (AQM) sites (2–17) were set up in each city as shown in Table 1. The citywide average concentrations were calculated by averaging the concentrations at all national AQM sites in each city (Wang et al., 2014). Gridded emissions data of nitrogen oxides (NO_x), SO_2, CO, PM and volatile organic compounds (VOC) from the 2012-based Multi-resolution Emission Inventory for China (MEIC, http://www.meicmodel.org/) (He, 2012; Zhang et al., 2009) were also collected.

2.2.2. Extinction coefficient

CALIPSO lidar is designed to acquire vertical profiles of extinction coefficient at two wavelengths (532 and 1064 nm) from a near nadir-viewing geometry during both day and night phases of the Sun-synchronous orbit, which has a 13:30 LT equatorial crossing time (Huang et al., 2009). The vertical profiles of extinction coefficient have been extensively used to measure the vertical distribution of aerosols (Koffi et al., 2012; Li and Han, 2016; Yu et al., 2010). In this study, the monthly mean aerosol extinction coefficient profiles of CALIPSO Level 3 version 3.00 with 60 m vertical resolution at 532 nm were used to investigate vertical distribution of PM in the Basin. Because the lidar observations in the nighttime are more accurate than those during the daytime, we only selected the aerosol extinction coefficient profiles from CALIPSO nighttime observations in cloud-free conditions (Yu et al., 2010) in this study. Atmospheric extinction coefficient profiles measured by EV-lidar in Chengdu (104.06°E, 30.70°N and 505 m above sea level) were also used to verify the PM vertical profiles in the Basin.

3. Results and discussion

3.1. Air quality overview

Featured by low altitudes (less than 500 m), high population, high urbanization rate, and a large number of vehicles (Table 1), all fifteen cities in the bottom zone of the Basin were subject to severe air pollution. The number of days with air quality exceeding Grade II standards at each of these cities was more than 20% during 2015 to 2016. Among these cities, CD was the most contaminated city by air pollution where there were 310 non-attainment days. MY had lowest non-attainment days at 149 days. Compared to the cities in the bottom zone, the non-attainment days in the three cities located in the slope zone, YA, BZ, and GW, ranged from 55 to 83 days. Their non-attainment rates were less than 12% of the annual total. The other two cities GZZ and ABZ, located in the edge zone of the Basin with high altitudes (about 3000 m), had merely 9 and 0 non-attainment days from 2015 to 2016, respectively.

Fig. 2 shows the differences of the non-attainment rates among the three zones or between different cities located in the same zone of the Basin. The non-attainment rates exhibited prominent seasonal variations in all 20 cities. Both worst air quality and the highest non-attainment rate can be identified in winter. There were 11 cities in the bottom zone with non-attainment rate exceeding 50% of the winter total (the highest was 72.93% in ZG). The second highest non-attainment rate can be found in spring in these cities across the Basin, excluding YA and GA. YA had the best air quality in spring. The reason is unknown yet and pending further analysis. In summer, air quality in most cities across the Basin was generally good and the non-attainment rate was relatively lower.

Table 1
Base information of the 20 cities across Sichuan Basin and their statistical results.

Part category		Population (million)	Altitude (m)	Urbanization rate	Possession of civil motor vehicles (million)	Number of AQM sites	Number of non-attainment days[a] January 1st, 2015–December 31th, 2016
Bottom of the basin	CD	14.66	481.00	71.47%	3.66.	8	310/728
	ZG	2.77	295.00	47.88%	0.16	4	270/728
	MS	3.00	411.00	41.87%	0.22	4	248/728
	LZ	4.29	250.00	46.08%	0.24	4	218/728
	DY	3.51	487.00	48.50%	0.36	4	215/728
	NJ	3.74	322.00	45.60%	0.16	4	209/728
	LS	3.26	370.00	47.31%	0.26	4	192/728
	DZ	5.57	277.00	40.87%	0.21	5	191/728
	YB	4.49	307.00	45.10%	0.22	6	180/728
	NC	6.36	273.00	43.80%	0.33	6	179/728
	ZY	3.57	355.00	39.50%	0.15	5	174/728
	GA	3.25	249.00	37.20%	0.14	5	163/728
	SN	3.29	276.00	45.90%	0.16	4	160/728
	CQ	30.17	161.00	60.94%	2.83	17	151/728
	MY	4.77	383.00	48.00%	0.43	4	149/728
Slope of the basin	YA	1.55	641.00	42.55%	0.13	4	83/728
	BZ	3.33	369.00	37.52%	0.14	4	83/728
	GY	2.63	927.00	40.80%	0.16	4	55/728
Edge of the basin	GZZ	1.16	2977.00	28.06%	0.08	2	9/721
	ABZ	0.93	3085.00	36.77%	0.10	3	0/717

[a] First digital number in the last column represents the total number of non-attainment days (>Grade II standards), and the second digital number stands for the total number of days.

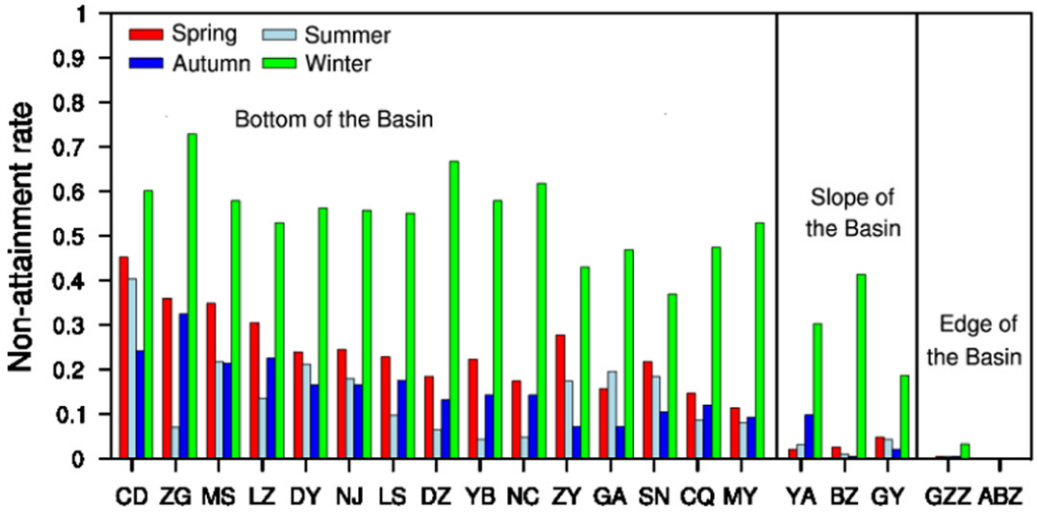

Fig. 2. Seasonal variation of non-attainment rates in the 20 cities across Sichuan Basin.

The six criteria air pollutants observed in the Basin were divided into two categories, i.e., the particulate matter (including $PM_{2.5}$ and PM_{10}) and the gaseous pollutants (including SO_2, NO_2, CO and O_3). Annual average concentrations of the six pollutants in the 20 cities are summarized in Table 2.

In the bottom zone, the annually averaged $PM_{2.5}$ concentrations ranged from 45 μg/m^3 (ZY) to 73 μg/m^3 (ZG) and regional annual average $PM_{2.5}$ concentration was about 55.87 μg/m^3. The both values exceeded the Grade II standard (35 μg/m^3). The annually averaged PM_{10} concentrations ranged from 76 μg/m^3 (MY) to 105 μg/m^3 (CD) and its regional annual average was 86.49 μg/m^3, also exceeding the Grade II standard of PM_{10} (70 μg/m^3). Compared to the bottom zone of the Basin, the annual average concentrations of PM were lower in the slope zone. The annually averaged $PM_{2.5}$ concentrations ranged from 25 μg/m^3 (GY) to 39 μg/m^3 (YA) and the regional annual average was 33.76 μg/m^3. Except for GY, the annual averages of $PM_{2.5}$ concentrations in the other cities in the slope zone also exceeded the Grade II standard. Likewise, the annually averaged PM_{10} concentrations ranged from 60 μg/m^3 (BZ) to 68 μg/m^3 (YA) in the slope zone with regional annual average 63.33 μg/m^3. These values were also greater than the Grade I standard (40 μg/m^3). The regional annual average concentrations of $PM_{2.5}$ and PM_{10} in the edge zone with cleaner air were only 19.71 μg/m^3 and 35.06 μg/m^3, respectively. Figs. 3a and b illustrate PM_{10} and $PM_{2.5}$ emissions in the Sichuan Basin. The lower emissions of $PM_{2.5}$ and PM_{10} are also observed in the edge zone, which make a partial contribution to the low PM concentrations over there.

The annual average concentrations of gaseous pollutants showed different spatial distributions compared to the particulate pollutants. Generally, the annual average concentrations of SO_2 in the 20 cities were lower than Grade II standard (60 μg/m^3, ~22.90 ppb). NO_2 levels in the air depend on the number of motor vehicles (Carr et al., 2002; Latham et al., 2001; Wang et al., 2010). There were 3.66 and 2.83 million civil vehicles in the mega cities of CD and CQ in the Basin in 2015, respectively (Table 1). As a result, high NO_x emissions can be also found in these two mega cities (see Fig. 3c). The annual average concentrations of NO_2 were 28 ppb and 24 ppb in the two cities, both exceeding Grade II standard (40 μg/m^3, ~21.28 ppb). The lowest annual average concentration (6 ppb) in the 20 cities was identified in ABZ in the edge zone with low NO_x emission (see Fig. 3c). The annual average concentrations of CO in four cities (CD, LS, DZ and CQ) of the bottom zone were higher than 900 ppb whereas the concentrations in the two edge zone cities were lower than 600 ppb. These concentration levels were in line with the spatial distribution of CO emission (see Fig. 3e). The highest annual average concentrations of O_3 were also monitored in

Table 2
Annual average concentrations of six criteria pollutants in the 20 cities across Sichuan Basin from 2015 to 2016.

Part category		$PM_{2.5}$	PM_{10}	SO_2	NO_2	CO	8 h O_3
		μg/m^3	μg/m^3	ppb	ppb	ppb	ppb
Bottom of the basin	CD	63 ± 38	105 ± 60	6 ± 2	28 ± 8.	981 ± 313	49 ± 28
	ZG	73 ± 45	104 ± 57	6 ± 3	18 ± 5	802 ± 314	36 ± 16
	MS	62 ± 35	94 ± 47	6 ± 3	17 ± 7	623 ± 262	49 ± 23
	LZ	62 ± 34	87 ± 49	7 ± 4	16 ± 5	530 ± 191	42 ± 22
	DY	53 ± 35	89 ± 50	5 ± 2	15 ± 7	856 ± 232	48 ± 23
	NJ	57 ± 37	80 ± 45	8 ± 4	15 ± 5	624 ± 254	48 ± 22
	LS	55 ± 34	80 ± 46	7 ± 4	18 ± 6	949 ± 269	43 ± 21
	DZ	59 ± 39	88 ± 51	4 ± 2	21 ± 5	943 ± 407	34 ± 17
	YB	57 ± 37	81 ± 47	8 ± 3	16 ± 5	798 ± 224	37 ± 17
	NC	59 ± 30	87 ± 43	5 ± 2	16 ± 6	753 ± 271	31 ± 16
	ZY	45 ± 31	87 ± 45	9 ± 7	10 ± 4	665 ± 242	52 ± 20
	GA	46 ± 33	80 ± 47	7 ± 3	12 ± 4	790 ± 235	45 ± 23
	SN	47 ± 27	77 ± 42	5 ± 2	13 ± 5	777 ± 219	45 ± 20
	CQ	54 ± 31	82 ± 41	6 ± 2	24 ± 7	902 ± 240	36 ± 23
	MY	48 ± 32	76 ± 45	5 ± 2	18 ± 6	800 ± 253	41 ± 20
Slope of the basin	YA	39 ± 25	68 ± 43	5 ± 2	14 ± 4	855 ± 352	33 ± 14
	BZ	37 ± 27	60 ± 39	2 ± 1	16 ± 5	887 ± 289	35 ± 17
	GY	25 ± 21	62 ± 40	8 ± 3	18 ± 7	671 ± 334	45 ± 19
Edge of the basin	GZZ	21 ± 9	37 ± 18	7 ± 4	14 ± 14	569 ± 213	30 ± 11
	ABZ	19 ± 6	33 ± 12	3 ± 2	6 ± 3	470 ± 238	34 ± 10

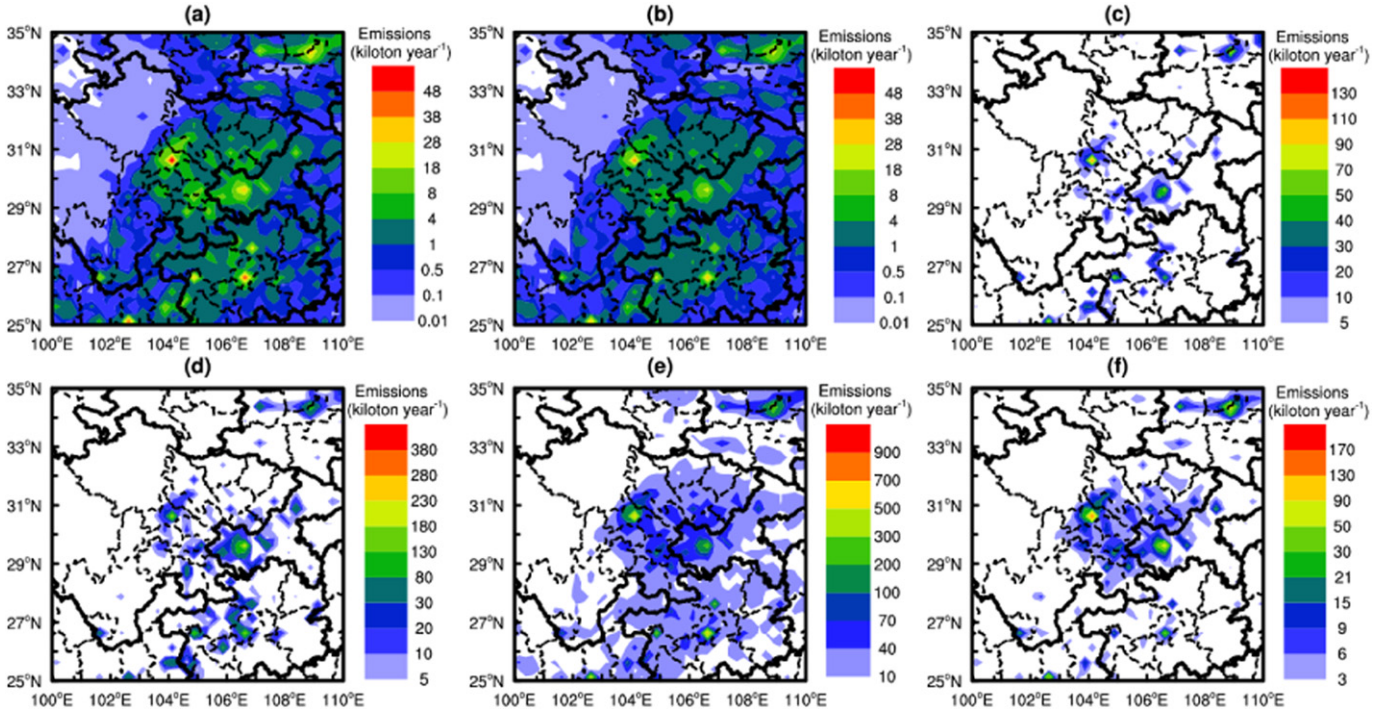

Fig. 3. Gridded emissions data of (a) PM_{10}, (b) $PM_{2.5}$, (c) NO_x, (d) SO_2, (e) CO and (f) VOC from the 2012-based MEIC inventory.

the bottom zone. The maximum and minimum concentrations of O_3 were 52 ppb in ZY and 30 ppb in GZZ, respectively. Overall, the higher concentrations of gaseous pollutants' concentrations mainly occurred in the bottom zoon and lower concentrations were observed in the cities of the edge zone, in line with the spatial distributions of their respective emissions (see Fig. 3).

In summary, $PM_{2.5}$ and PM_{10} concentrations decreased roughly with increasing altitude in the Sichuan Basin. The annual average concentrations of PM differed in the three zones significantly, but gaseous pollutants seemed not to exhibit considerable differences among the three zones. The average concentration of each gaseous pollutant varied among cities in the same zone of the Basin. This indicates that the difference of energy structures among cities across the Basin is significant. The spatial patterns of PM and gaseous pollutants in the Sichuan Basin differ from the North China Plain where high concentrations of particulate and gaseous pollutants are monitored in the same industrialized and densely populated city cluster (Pui et al., 2014; Wang et al., 2014; Zhang et al., 2009; Zhao et al., 2011).

3.2. Primary pollutant

A daily 'primary pollutant' is defined to measure one of six criteria air pollutants contributing the most to the poor air quality (Wang et al., 2014). The primary pollutant showed significant variations among the three zones of the Sichuan Basin. Seasonal changes in primary pollutants were also significant in the same zone of the Basin. Table 3 presents the fractions of each measured air pollutant as the primary pollutant in each season.

As shown, the primary pollutant in the bottom and slope zones of the Basin was $PM_{2.5}$, which contributed to 77.83% of the non-attainment days throughout the year. In particular, $PM_{2.5}$ contributed to more than 93% non-attainment days in winter. According to these results, more efforts should be made to control $PM_{2.5}$ so as to improve air quality in the Basin. However, in the edge zone of the Basin, NO_2 became the primary pollutant in most of the year except for spring due to relatively low level of PM. The low emissions of PM, precursor gases, and VOC were also found in the edge zone (see Fig. 3). Large difference of altitudes between the edge and the bottom zone (~2500 m) retards atmospheric transport of particulate pollutants from the bottom to the edge zone (Emeis and Schäfer, 2006; Tennekes, 1973). Hence, both low emission and weak atmospheric transport are conducive to forming the low concentrations of particulate pollutants in the edge zone.

In spring, PM_{10} as the primary pollutant in the slope and edge zones contributed 61.11% and 100% to the non-attainment days, respectively. However, in the bottom zone $PM_{2.5}$ was the primary pollutant whereas PM_{10} was ranked as the third primary pollutant, only contributing 1.86% to the annual total non-attainment day. This feature differs from north or northwest China where the air quality is significantly affected by dust weather (Qu et al., 2010; Shen et al., 2014; Tao et al., 2012). PM_{10} as the primary pollutant in north and northwest China contributed 23.6% to annual non-attainment days and 46.9% to spring non-attainment days (Wang et al., 2014). The effects of particulate matter emission and complex terrain on primary pollutant were also analyzed. The results show that fine particulates are dominant in PM emissions (see Figs. 3a and b) and the dust from north China are seldom transported into the bottom zone of the Basin due to its complex mountainous topography (Chen et al., 2015; Liao et al., 2016). These two factors are not conducive to PM_{10} as the primary pollutant in the bottom

Table 3
Annual and seasonal contributions of six pollutants as the primary pollutant to non-attainment days in the three zones of Sichuan Basin.

Part category		$PM_{2.5}$	PM_{10}	SO_2	NO_2	CO	8 h O_3
Bottom of the basin	Annual	79.49%	1.86%	0.00%	0.07%	0.00%	18.78%
	Spring	71.56%	4.74%	0.00%	0.30%	0.00%	24.00%
	Summer	11.14%	0.25%	0.00%	0.00%	0.00%	88.86%
	Autumn	88.74%	1.15%	0.00%	0.00%	0.00%	10.11%
	Winter	98.86%	1.20%	0.00%	0.00%	0.00%	0.00%
Slope of the basin	Annual	77.83%	12.67%	0.00%	0.00%	0.00%	9.95%
	Spring	11.11%	61.11%	0.00%	0.00%	0.00%	27.78%
	Summer	0.00%	0.00%	0.00%	0.00%	0.00%	100%
	Autumn	73.91%	21.74%	0.00%	0.00%	0.00%	4.35%
	Winter	93.29%	7.32%	0.00%	0.00%	0.00%	0.00%
Edge of the basin	Annual	0.00%	22.22%	0.00%	77.78%	0.00%	0.00%
	Spring	0.00%	100%	0.00%	0.00%	0.00%	0.00%
	Summer	0.00%	0.00%	0.00%	100%	0.00%	0.00%
	Autumn	0.00%	0.00%	0.00%	100%	0.00%	0.00%
	Winter	0.00%	16.67%	0.00%	83.33%	0.00%	0.00%

zone of the Basin. However, PM_{10} as the primary pollutant accounted for 4.74% of total non-attainment days in the bottom zone in spring. This indicates that the air quality over the Basin is not affected by dust from northwest China markedly (Tao et al., 2013b; Zhao et al., 2010). In summer, O_3 as the primary pollutant in the bottom and slope zones contributed more than 88% to the non-attainment days. In the edge zone, O_3 as primary pollutant has never been found which might be related to low temperature and low emissions of NOx and VOC (see Figs. 3c and f) (Atkinson, 2000; Li et al., 2012; Li et al., 2016; Pudasainee et al., 2006).

3.3. Changes in air pollutants with altitude

3.3.1. PM

As shown in Table 2, $PM_{2.5}$ and PM_{10} concentrations in the Sichuan Basin decreased with increasing altitude. To understand the variation characteristics of $PM_{2.5}$ and PM_{10} concentrations with altitude, daily mean $PM_{2.5}$ and PM_{10} concentrations and the corresponding altitudes of 15 cities in the bottom zone, 3 cities in the slope zone, and 2 cities in the edge zone were averaged to calculate their respective seasonal and annual average. The changes in the average $PM_{2.5}$ and PM_{10} concentrations with altitudes were then fitted by polynomials on seasonal or annual timescale, respectively (Fig. 4).

As shown in Fig. 4, there are nonlinear relationships between y (air concentrations of $PM_{2.5}$ and PM_{10}) and x (altitude), given by $y = (a + b/x)^2$ which can be applied to the altitude below 3300 m. Model coefficients, a and b change by season, as shown in Fig. 4. The fitting curves show that the decreasing rates of $PM_{2.5}$ and PM_{10} concentrations with altitude in the bottom zone are much bigger than those in the slope zone of the Basin. As also seen, the fitting curves become steep and tend to slowly changed from the slope zone to the edge zone of the Basin. This feature suggests that the high concentrations of particulate pollutants mostly lay within the lower atmospheric boundary layer of the Basin. Significant differences of particulate pollutant concentrations among different seasons were observed and these differences decreased with increasing altitude remarkably, as shown in Fig. 4.

Previous studies showed that particulate pollutants made largest contributions to atmospheric extinction coefficient in urban areas (Charlson, 1969; Sabetghadam and Ahmadi-Givi, 2014). To verify the fitting results, the monthly mean aerosol extinction coefficient profiles from CALIPSO observations at 532 nm from January 2015 to November 2016 are illustrated in Fig. 5. It can be seen that the aerosol extinction coefficient declined rapidly below the 1000 m height but is slowly altered above the 1000 m height, showing the similar vertical profiles with PM profiles (Fig. 4). The aerosol extinction coefficient profiles in different seasons also differ significantly. These results indicate that the nonlinear relationship $y = (a + b/x)^2$ provides a good fit to the vertical distribution of particulate pollutants in the Basin.

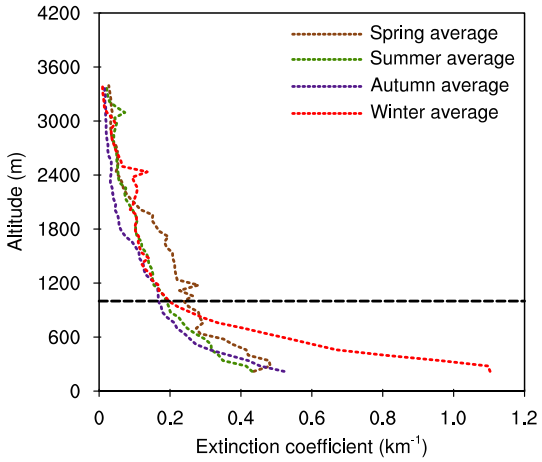

Fig. 5. Seasonal averaging aerosol extinction coefficient profiles observed at 532 nm in the bottom zone of the Basin (107.5°E, 30°N) at the height about 200 m from CALIPSO observations. The dashed black line represents 1000 m height.

Atmospheric extinction coefficient profiles measured by EV-lidar in Chengdu were also adopted to verify the fitted PM profiles. EV-lidar derived atmospheric extinction coefficient vertical profiles in selected autumn and winter days are shown in Fig. 6. Heavy pollution of PM_{10} and $PM_{2.5}$ concentrations occurred in these selected days during which PM_{10} concentrations and $PM_{2.5}$ concentrations were greater than 200 μg/m^3 and 150 μg/m^3, respectively. It is worth noting that the aerosol extinction coefficients from CALIPSO observed in rural area corresponded to low concentrations of particulate pollutants. Accordingly, the aerosol extinction coefficients from the EV-lidar in Chengdu (Fig. 6) were much bigger than those from CALIPSO observations (Fig. 5).

Although the atmospheric extinction coefficient in Fig. 6 was obtained by transient observations, they are very similar to the aerosol extinction coefficient profiles from CALIPSO. Both profiles are also similar to the fitting results presented in Fig. 4. It can be also identified that the vertical thickness of high particulate pollutant concentrations in the Basin is less than 500 m (Fig. 6), which could enhance our understanding of the vertical distribution of particulate pollutants in the Basin and provide important scientific evidence in the mitigation and control of particulate pollutants.

3.3.2. Gaseous pollutant

Gaseous pollutants were also fitted by altitudes using the same approach as for PM results displayed in Fig. 7.

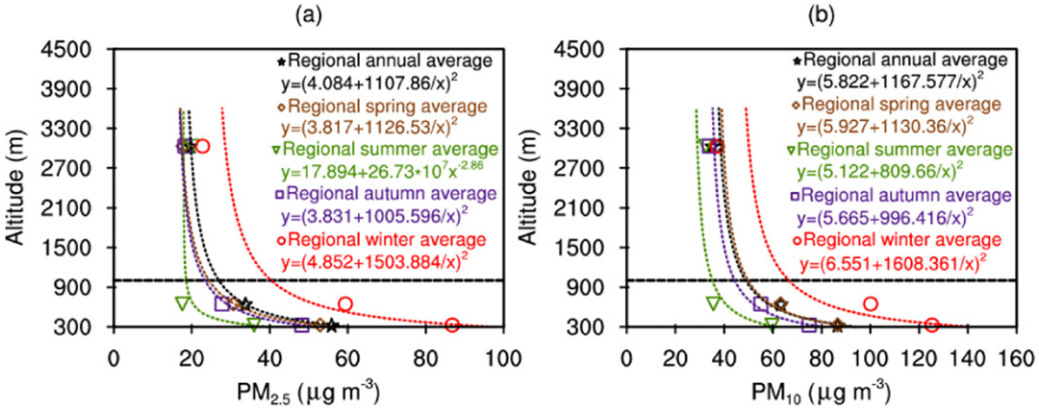

Fig. 4. Annual and seasonal concentrations of (a) $PM_{2.5}$ and (b) PM_{10} in the three zones of the Sichuan Basin and their changes with altitude. The dotted lines are the fitting curves of particulate pollutants concentrations with altitude. Black dashed line indicates the 1000 m height.

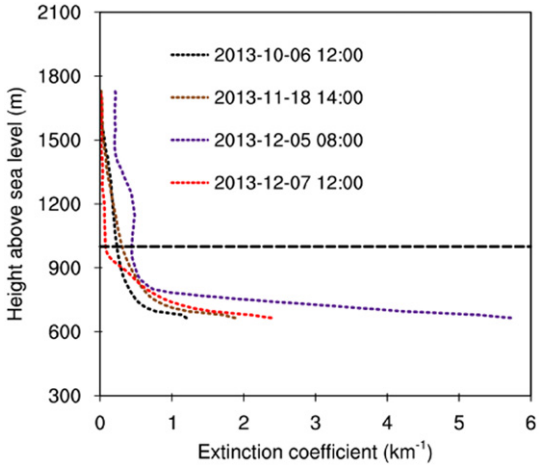

Fig. 6. Atmospheric extinction coefficient profiles from EV-lidar measured in Chengdu at 12:00 BJT on October 6th, 2013; 14:00 BJT on November 18th, 2013; 08:00 BJT on December 5th, 2013 and 12:00 BJT on December 7th, 2013. The black dashed line represents the 1000 m height.

As shown, the seasonal difference of SO_2 concentration between the bottom and slope zones of Sichuan Basin was small but in the edge zone this difference was big. This contrasted to the seasonal difference of particulate pollutant concentrations (Fig. 4). The seasonal differences of NO_2 concentrations in the three zones were all insignificant. Seasonal differences of the other two gaseous pollutants O_3 and CO concentrations were similar to particulate pollutant concentrations, showing large differences in the bottom or slope zones but small in the edge zone. There are no solid relationships between annual or seasonal average concentrations of the four gaseous pollutants and altitude.

3.4. Horizontal homogeneities of air pollutants

The Pearson correlation analysis for daily air concentrations of six air pollutants between different cities was performed to assess the differences of air pollutants between cities in the bottom zone of the Sichuan Basin. Table 4 shows the correlation coefficients (r) for daily $PM_{2.5}$ and PM_{10} concentrations between cities in the bottom zone of the Basin from January 2015 to November 2016.

As seen from Table 4, all paired cities showed positive correlations, and the correlation coefficients of $PM_{2.5}$ and PM_{10} were greater than those of gaseous pollutants SO_2, NO_2, O_3 and CO (results not shown), indicating that particulate pollutants have broader regional distribution than gaseous pollutants which are significantly limited by their local emissions. It is interesting to note that all correlation coefficients of particulate pollutants between cities are greater than 0.65 and even reaching over 0.9 in some paired cities. These correlation coefficients were greater than those in the NCP and YRD, respectively (see Tables S1 and S2), suggesting stronger horizontal homogeneities of the particulate pollutants across the bottom zone of the Basin as compared with the NCP and YRD. Such horizontal homogeneity may be related to the spatial distribution of emissions, the closed terrain, and unique meteorological conditions. As shown in Fig. 3, the stronger emissions of precursor gases, VOC, and PM occur in the bottom zone of the Sichuan Basin. The other large emission sources are located outside of the Basin which unlikely affect the air quality in the bottom zone because Yunnan-Guizhou plateau and Qinling-Daba Mountains block the atmospheric transport of these air pollutants into the Basin (Fig. 3). Likewise, particulate pollutants from the Basin also could not be transported out of the Basin due to the closed terrain and local meteorological conditions, leading to the horizontal homogeneity of particulate pollutants in the bottom zone of the Basin.

To further elucidate the changes in the horizontal homogeneities of the targeted air pollutants in the three zones of the Sichuan Basin, a

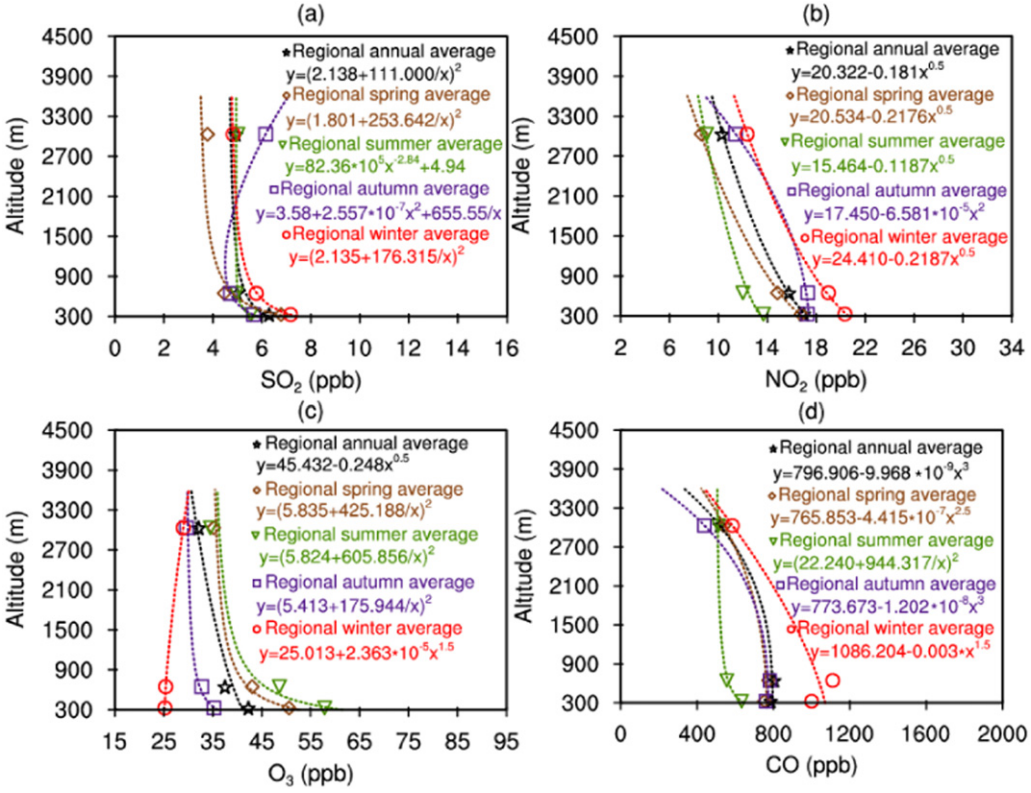

Fig. 7. Annual and seasonal concentrations of (a) SO_2, (b) NO_2, (c) O_3 and (d) CO in the three zones of Sichuan Basin, and their variations with altitude, respectively. The dotted lines are the fitting curves of gaseous pollutant concentrations with altitude.

Table 4
Pearson correlation coefficients of $PM_{2.5}$ (cells above the diagonal) and of PM_{10} (cells bellow the diagonal) between cities in the bottom zone of Sichuan Basin.

	CD	ZG	MS	LZ	DY	NJ	LS	DZ	YB	NC	ZY	GA	SN	CQ	MY
CD		0.84	0.91	0.74	0.92	0.81	0.85	0.74	0.82	0.81	0.79	0.74	0.80	0.72	0.88
ZG	0.82		0.86	0.87	0.82	0.93	0.88	0.74	0.91	0.85	0.87	0.79	0.88	0.76	0.81
MS	0.91	0.85		0.78	0.85	0.84	0.89	0.73	0.85	0.79	0.80	0.72	0.81	0.71	0.82
LZ	0.75	0.89	0.79		0.69	0.85	0.77	0.71	0.86	0.77	0.78	0.78	0.83	0.82	0.68
DY	0.90	0.79	0.84	0.71		0.80	0.81	0.77	0.79	0.83	0.75	0.75	0.80	0.73	0.95
NJ	0.80	0.93	0.84	0.88	0.79		0.83	0.77	0.86	0.87	0.88	0.81	0.91	0.79	0.77
LS	0.84	0.86	0.89	0.79	0.78	0.81		0.72	0.86	0.78	0.79	0.73	0.80	0.69	0.79
DZ	0.73	0.74	0.72	0.73	0.76	0.76	0.7		0.77	0.89	0.72	0.89	0.84	0.84	0.77
YB	0.80	0.91	0.84	0.90	0.74	0.86	0.85	0.75		0.83	0.81	0.79	0.83	0.76	0.77
NC	0.79	0.85	0.78	0.77	0.82	0.87	0.75	0.86	0.80		0.83	0.92	0.94	0.83	0.84
ZY	0.83	0.88	0.85	0.79	0.81	0.89	0.81	0.74	0.81	0.83		0.78	0.86	0.72	0.75
GA	0.73	0.78	0.72	0.79	0.75	0.82	0.71	0.89	0.77	0.89	0.76		0.88	0.90	0.76
SN	0.77	0.86	0.78	0.81	0.78	0.90	0.75	0.80	0.81	0.94	0.82	0.86		0.82	0.80
CQ	0.70	0.77	0.71	0.82	0.71	0.80	0.67	0.82	0.76	0.81	0.71	0.89	0.81		0.71
MY	0.87	0.78	0.81	0.68	0.94	0.76	0.76	0.76	0.73	0.83	0.82	0.72	0.77	0.67	

homogeneity index HI was defined as a measurement of regional horizontal homogeneity of air pollutants, given by

$$HI = (r_1 + r_2 + r_3 + \cdots + r_n)/n,$$

where r_i is a correlation coefficient of daily air pollutant concentrations between a paired city in the Basin with statistical significance of 0.05, n is the number of paired city. A large value of HI represents the strong horizontal homogeneities of the air pollutants in the Basin. The seasonal changes in the horizontal homogeneities of the six criteria air pollutant in the three zones of the Basin are shown in Fig. 8.

As shown in Fig. 8, most HI values in the three zones of the Basin were positive, indicating significant horizontal homogeneities of the targeted air pollutants across the Basin. Overall, the horizontal homogeneities of these air pollutants were strong in the bottom zone, moderate in the slope zone, and weak in the edge zone, except for SO_2. The horizontal homogeneities of the targeted air pollutants also exhibited significant seasonal variations. In the bottom zone, the large HI values of $PM_{2.5}$, PM_{10} and SO_2 were found in winter, O_3 and CO in autumn, and NO_2 in spring. The smallest HI values of the targeted pollutants were found in summer, except for O_3. Similar seasonal changes in the horizontal homogeneities of those air pollutants were discerned in the slope zone, except for SO_2. The HI values of most air pollutants excluding SO_2 in the edge zone were relatively small in which the most HI values for O_3 were negative. Particularly, the horizontal homogeneity values of $PM_{2.5}$ and PM_{10} were much higher than those of gaseous pollutants. Especially, the HI values of the particulate pollutants were as high as 0.8 in winter. These results are consistent with their respective correlation coefficients as aforementioned above. The strong horizontal homogeneity of particulate pollutants in the bottom zone of the Basin suggests that the joint efforts and control measures by all cities could be made to improve the regional air quality across the Sichuan Basin.

4. Conclusions

The distribution of six criteria air pollutants in 20 cities in the three zones across the Sichuan Basin and their temporal variations were investigated from January 1st, 2015 to December 31th, 2016. Results revealed heavy air pollution in the bottom zone of the Basin, moderate pollution in the slope zone, and weak pollution in the edge zone. Substantial differences of the primary pollutant among the three zones were observed. It was found that $PM_{2.5}$ and O_3 were the first and second

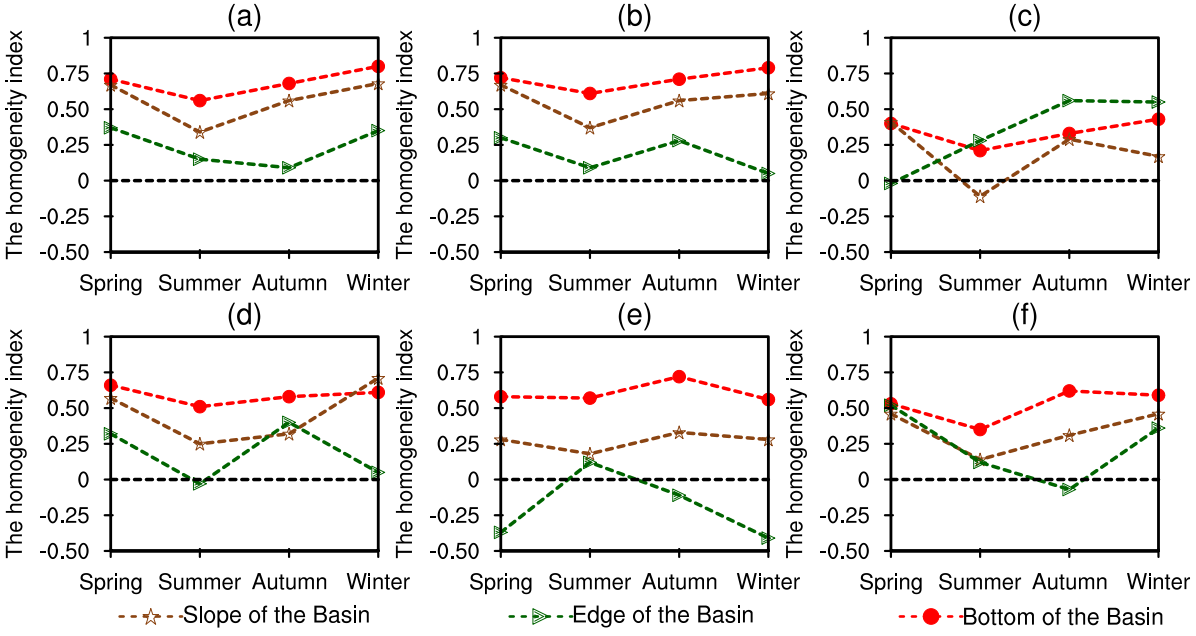

Fig. 8. Seasonal changes in the horizontal homogeneities of (a) $PM_{2.5}$, (b) PM_{10}, (c) SO_2, (d) NO_2, (e) O_3, and (f) CO in the three zones of the Sichuan Basin. The black dashed line represents the zero of the index.

primary pollutant in the bottom zone, and $PM_{2.5}$ and PM_{10} were the first and second primary pollutant in the slope zone, respectively. In the edge zone, however, NO_2 often became the primary pollutant.

Six criteria air pollutants ($PM_{2.5}$, PM_{10}, SO_2, NO_2, CO and 1 h O_3) were divided into two categories of particulate matter and gaseous pollutants. In the Sichuan Basin, concentrations of particulate matter decrease dramatically with increasing altitude which were fitted by a nonlinear functional relationship $y = (a + b / x)^2$. This nonlinear function has been validated by the extinction coefficient profiles from CALIPSO observations and measured by EV-lidar, and can be used to reflect the vertical distribution of particulate matter concentrations in the Basin. The distribution of particulate matter concentrations showed more significant horizontal homogeneities as compared with that in the North China Plain and Yangtze River Delta. Unlike particulate matter, gaseous pollutant concentrations exhibited diverse variations with altitude, showing the increase with altitude in some seasons but decrease with altitude in other seasons. The horizontal homogeneities of gaseous pollutants were also not as strong as those of particulate pollutants. The results from the present study provide an important scientific basis for understanding the temporal-spatial pattern and variability of air pollution in the Sichuan Basin.

Conflict of interest

We declare that all authors have no competing interests.

Acknowledgements

This work was supported by the National Natural Science Foundation of China (91644226 and 41205008), the Fundamental Research Funds for the Central Universities (lzujbky-2017-it20) and the National Key Research Project of China-Strategy on Black Carbon Reduction and Evaluation of Health Effects of Climate Change (2016YFA0602004). This work was also supported by the CALIPSO program. The CALIPSO data were obtained from the NASA Langley Research Center Atmospheric Sciences Data Center. The authors also thank Tsinghua University for providing MEIC data products. Anonymous reviewers who provided comments and suggestions are gratefully acknowledged.

Appendix A. Supplementary data

Supplementary data to this article can be found online at http://dx.doi.org/10.1016/j.scitotenv.2017.08.205.

References

Atkinson, R., 2000. Atmospheric chemistry of VOCs and NOx. Atmos. Environ. 34, 2063–2101.
Battelle Memorial Institute, Center for International Earth Science Information Network - CIESIN - Columbia University, 2013. Global Annual Average $PM_{2.5}$ Grids From MODIS and MISR Aerosol Optical Depth (AOD). NASA Socioeconomic Data and Applications Center (SEDAC), Palisades, NY.
Boznar, M., Lesjak, M., Mlakar, P., 1993. A neural network-based method for short-term predictions of ambient SO_2 concentrations in highly polluted industrial areas of complex terrain. Atmos. Environ. Part B 27, 221–230.
Brauer, M., Amann, M., Burnett, R.T., Cohen, A., Dentener, F., Ezzati, M., et al., 2012. Exposure assessment for estimation of the global burden of disease attributable to outdoor air pollution. Environ. Sci. Technol. 46, 652–660.
Carr, D., von Ehrenstein, O., Weiland, S., Wagner, C., Wellie, O., Nicolai, T., et al., 2002. Modeling annual benzene, toluene, NO_2, and soot concentrations on the basis of road traffic characteristics. Environ. Res. 90, 111–118.
Charlson, R.J., 1969. Atmospheric visibility related to aerosol mass concentration: review. Environ. Sci. Technol. 3, 913–918.
Chen, Y., Xie, S., 2012. Temporal and spatial visibility trends in the Sichuan Basin, China, 1973 to 2010. Atmos. Res. 112, 25–34.
Chen, Y., Xie, S., Luo, B., Zhai, C., 2014. Characteristics and origins of carbonaceous aerosol in the Sichuan Basin, China. Atmos. Environ. 94, 215–223.
Chen, Y., Luo, B., Xie, S.-d., 2015. Characteristics of the long-range transport dust events in Chengdu, Southwest China. Atmos. Environ. 122, 713–722.
Chen, Y., Xie, S.-d., Luo, B., Zhai, C.-z., 2017. Particulate pollution in urban Chongqing of southwest China: historical trends of variation, chemical characteristics and source apportionment. Sci. Total Environ. 584–585, 523–534.
Deng, T., Wu, D., Deng, X., Tan, H., Li, F., Liao, B., 2014. A vertical sounding of severe haze process in Guangzhou area. Sci. China Earth Sci. 57, 2650–2656.
Emeis, S., Schäfer, K., 2006. Remote sensing methods to investigate boundary-layer structures relevant to air pollution in cities. Bound.-Layer Meteorol. 121, 377–385.
Fang, M., Chan, C.K., Yao, X., 2009. Managing air quality in a rapidly developing nation: China. Atmos. Environ. 43, 79–86.
Guo, Y., Zeng, H., Zheng, R., Li, S., Barnett, A.G., Zhang, S., et al., 2016. The association between lung cancer incidence and ambient air pollution in China: a spatiotemporal analysis. Environ. Res. 144 (Part A), 60–65.
Gustin, M.S., Fine, R., Miller, M., Jaffe, D., Burley, J., 2015. The Nevada Rural Ozone Initiative (NVROI): insights to understanding air pollution in complex terrain. Sci. Total Environ. 530–531, 455–470.
He, K., 2012. Multi-Resolution Emission Inventory for China (MEIC): Model Framework and 1990–2010 Anthropogenic Emissions, AGU Fall Meeting Abstracts.
He, Q., Guo, W., Zhang, G., Yan, Y., Chen, L., 2015. Characteristics and seasonal variations of carbonaceous species in $PM_{2.5}$ in Taiyuan, China. Atmosphere 6, 850.
Hu, X.-M., Ma, Z., Lin, W., Zhang, H., Hu, J., Wang, Y., et al., 2014. Impact of the Loess Plateau on the atmospheric boundary layer structure and air quality in the North China Plain: a case study. Sci. Total Environ. 499, 228–237.
Huang, J., Fu, Q., Su, J., Tang, Q., Minnis, P., Hu, Y., et al., 2009. Taklimakan dust aerosol radiative heating derived from CALIPSO observations using the Fu-Liou radiation model with CERES constraints. Atmos. Chem. Phys. 9, 4011–4021.
Huang, Q., Cai, X., Song, Y., Zhu, T., 2017. Air stagnation in China (1985–2014): climatological mean features and trends. Atmos. Chem. Phys. 17, 7793–7805.
Jazcilevich, A.D., García, A.R., Caetano, E., 2005. Locally induced surface air confluence by complex terrain and its effects on air pollution in the valley of Mexico. Atmos. Environ. 39, 5481–5489.
Koffi, B., Schulz, M., Bréon, F.-M., Griesfeller, J., Winker, D., Balkanski, Y., et al., 2012. Application of the CALIOP layer product to evaluate the vertical distribution of aerosols estimated by global models: AeroCom phase I results. J. Geophys. Res.-Atmos. 117 (n/a-n/a).
Langrish, J.P., Li, X., Wang, S., Lee, M.M.Y., Barnes, G.D., Miller, M.R., et al., 2012. Reducing personal exposure to particulate air pollution improves cardiovascular health in patients with coronary heart disease. Environ. Health Perspect. 120, 367–372.
Latham, S., Kollamthodi, S., Boulter, P., Nelson, P., Hickman, A., 2001. Assessment of Primary NO_2 Emissions, Hydrocarbon Speciation and Particulate Sizing on a Range of Road Vehicles. TRL.
Li, J., Han, Z., 2016. Aerosol vertical distribution over east China from RIEMS-Chem simulation in comparison with CALIPSO measurements. Atmos. Environ. 143, 177–189.
Li, J., Zhang, H., Ying, Q., 2012. Comparison of the SAPRC07 and SAPRC99 photochemical mechanisms during a high ozone episode in Texas: differences in concentrations, OH budget and relative response factors. Atmos. Environ. 54, 25–35.
Li, Y., Chen, Q., Zhao, H., Wang, L., Tao, R., 2015. Variations in PM_{10}, $PM_{2.5}$ and $PM_{1.0}$ in an urban area of the Sichuan Basin and their relation to meteorological factors. Atmosphere 6, 150.
Li, L., An, J.Y., Shi, Y.Y., Zhou, M., Yan, R.S., Huang, C., et al., 2016. Source apportionment of surface ozone in the Yangtze River Delta, China in the summer of 2013. Atmos. Environ. 144, 194–207.
Li, Q., Wang, E., Zhang, T., Hu, H., 2017. Spatial and temporal patterns of air pollution in Chinese cities. Water Air Soil Pollut. 228, 92.
Liao, Q., Luo, B., Du, Y., Liu, P., Zhang, W., Cao, P., et al., 2016. Effects and characteristics of floating dust weather on air quality in Sichuan Basin. Environ. Monit. China 32, 51–55 (in Chinese).
Liao, T., Wang, S., Ai, J., Gui, K., Duan, B., Zhao, Q., et al., 2017. Heavy pollution episodes, transport pathways and potential sources of $PM_{2.5}$ during the winter of 2013 in Chengdu (China). Sci. Total Environ. 584–585, 1056–1065.
Liu, H., Wang, X., Zhang, J., He, K., Wu, Y., Xu, J., 2013. Emission controls and changes in air quality in Guangzhou during the Asian Games. Atmos. Environ. 76, 81–93.
Luo Yunfeng, L.W., Xiuji, Zhou, He, Qing, Jizu, Qing, 2000. Analysis of the atmospheric aerosol optical depth over China in 1980s. J. Meteor. Res. 14, 490–502.
Miao, Y., Liu, S., Zheng, Y., Wang, S., Chen, B., 2015. Numerical study of the effects of topography and urbanization on the local atmospheric circulations over the Beijing-Tianjin-Hebei, China. Adv. Meteorol. 2015.
Niu, S., Lu, C., Yu, H., Zhao, L., Lü, J., 2010. Fog research in China: an overview. Adv. Atmos. Sci. 27, 639–662.
Pope, C.A., Dockery, D.W., 2006. Health effects of fine particulate air pollution: lines that connect. J. Air Waste Manage. Assoc. 56, 709–742.
Pudasainee, D., Sapkota, B., Shrestha, M.L., Kaga, A., Kondo, A., Inoue, Y., 2006. Ground level ozone concentrations and its association with NOx and meteorological parameters in Kathmandu valley, Nepal. Atmos. Environ. 40, 8081–8087.
Pui, D.Y.H., Chen, S.-C., Zuo, Z., 2014. $PM_{2.5}$ in China: measurements, sources, visibility and health effects, and mitigation. Particuology 13, 1–26.
Qu, W.J., Arimoto, R., Zhang, X.Y., Zhao, C.H., Wang, Y.Q., Sheng, L.F., et al., 2010. Spatial distribution and interannual variation of surface PM_{10} concentrations over eighty-six Chinese cities. Atmos. Chem. Phys. 10, 5641–5662.
Sabetghadam, S., Ahmadi-Givi, F., 2014. Relationship of extinction coefficient, air pollution, and meteorological parameters in an urban area during 2007 to 2009. Environ. Sci. Pollut. Res. 21, 538–547.
Saide, P.E., Carmichael, G.R., Spak, S.N., Gallardo, L., Osses, A.E., Mena-Carrasco, M.A., et al., 2011. Forecasting urban PM_{10} and $PM_{2.5}$ pollution episodes in very stable nocturnal conditions and complex terrain using WRF–Chem CO tracer model. Atmos. Environ. 45, 2769–2780.
Shen, Z., Cao, J., Zhang, L., Liu, L., Zhang, Q., Li, J., et al., 2014. Day–night differences and seasonal variations of chemical species in PM_{10} over Xi'an, northwest China. Environ. Sci. Pollut. Res. 21, 3697–3705.

Tao, M., Chen, L., Su, L., Tao, J., 2012. Satellite observation of regional haze pollution over the North China Plain. J. Geophys. Res.-Atmos. 117 (n/a-n/a).
Tao, J., Cheng, T., Zhang, R., Cao, J., Zhu, L., Wang, Q., et al., 2013a. Chemical composition of $PM_{2.5}$ at an urban site of Chengdu in southwestern China. Adv. Atmos. Sci. 30, 1070–1084.
Tao, J., Zhang, L., Engling, G., Zhang, R., Yang, Y., Cao, J., et al., 2013b. Chemical composition of $PM_{2.5}$ in an urban environment in Chengdu, China: importance of springtime dust storms and biomass burning. Atmos. Res. 122, 270–283.
Tao, M., Chen, L., Xiong, X., Zhang, M., Ma, P., Tao, J., et al., 2014. Formation process of the widespread extreme haze pollution over northern China in January 2013: implications for regional air quality and climate. Atmos. Environ. 98, 417–425.
Tennekes, H., 1973. A model for the dynamics of the inversion above a convective boundary layer. J. Atmos. Sci. 30, 558–567.
Wang, Q.-W., Tan, Z.-M., 2014. Multi-scale topographic control of southwest vortex formation in Tibetan Plateau region in an idealized simulation. J. Geophys. Res.-Atmos. 119, 11,543–511,561.
Wang, X., Zhang, Y., Hu, Y., Zhou, W., Lu, K., Zhong, L., et al., 2010. Process analysis and sensitivity study of regional ozone formation over the Pearl River Delta, China, during the PRIDE-PRD2004 campaign using the community multiscale air quality modeling system. Atmos. Chem. Phys. 10, 4423–4437.
Wang, Y., Ying, Q., Hu, J., Zhang, H., 2014. Spatial and temporal variations of six criteria air pollutants in 31 provincial capital cities in China during 2013–2014. Environ. Int. 73, 413–422.
Wang, X., Dickinson, R.E., Su, L., Zhou, C., Wang, K., 2017. $PM_{2.5}$ pollution in China and how it has been exacerbated by terrain and meteorological conditions. Bull. Am. Meteorol. Soc. http://dx.doi.org/10.1175/BAMS-D-16-0301.1 (in press).
Xu, J., Chang, L., Qu, Y., Yan, F., Wang, F., Fu, Q., 2016. The meteorological modulation on $PM_{2.5}$ interannual oscillation during 2013 to 2015 in Shanghai, China. Sci. Total Environ. 572, 1138–1149.
Yim, S.H.L., Fung, J.C.H., Ng, E.Y.Y., 2014. An assessment indicator for air ventilation and pollutant dispersion potential in an urban canopy with complex natural terrain and significant wind variations. Atmos. Environ. 94, 297–306.
Yu, H., Chin, M., Winker, D.M., Omar, A.H., Liu, Z., Kittaka, C., et al., 2010. Global view of aerosol vertical distributions from CALIPSO lidar measurements and GOCART simulations: regional and seasonal variations. J. Geophys. Res.-Atmos. 115.
Yu, S., Gao, W., Xiao, D., Peng, J., 2016. Observational facts regarding the joint activities of the southwest vortex and plateau vortex after its departure from the Tibetan Plateau. Adv. Atmos. Sci. 33, 34–46.
Zhang, Q., Streets, D.G., Carmichael, G.R., He, K., Huo, H., Kannari, A., et al., 2009. Asian emissions in 2006 for the NASA INTEX-B mission. Atmos. Chem. Phys. 9, 5131–5153.
Zhang, X.Y., Wang, Y.Q., Niu, T., Zhang, X.C., Gong, S.L., Zhang, Y.M., et al., 2012. Atmospheric aerosol compositions in China: spatial/temporal variability, chemical signature, regional haze distribution and comparisons with global aerosols. Atmos. Chem. Phys. 12, 779–799.
Zhang, J., Luo, B., Zhang, J., Ouyang, F., Song, H., Liu, P., et al., 2017. Analysis of the characteristics of single atmospheric particles in Chengdu using single particle mass spectrometry. Atmos. Environ. 157, 91–100.
Zhao, Q., He, K., Rahn, K., Ma, Y., Jia, Y., Yang, F., et al., 2010. Dust storms come to Central and Southwestern China, too: implications from a major dust event in Chongqing. Atmos. Chem. Phys. 10, 2615–2630.
Zhao, Y., Nielsen, C., Lei, Y., McElroy, M., Hao, J., 2011. Quantifying the uncertainties of a bottom-up emission inventory of anthropogenic atmospheric pollutants in China. Atmos. Chem. Phys. 11, 2295–2308.
Zhao, S., Yu, Y., Yin, D., He, J., 2015. Meteorological dependence of particle number concentrations in an urban area of complex terrain, Northwestern China. Atmos. Res. 164, 304–317.